Modal reduction for a problem of heat transfer with radiation in an enclosure

Benjamin Gaume, Frédéric Joly, Olivier Quéméner

Modal reduction for a problem of heat transfer with radiation in an enclosure

B. Gaume[a,*], F. Joly[a], O. Quéméner[a]

[a] *LMEE, Univ Evry, Université Paris-Saclay, 91020, Evry, France.*

Abstract

We propose an original method to reduce a radiation dominated heat transfer problem. To that end, the Amalgam Reduced Order Modal Model (AROMM) method, which preserves the integrity of the geometry, is coupled to the classical radiosity method. The treated application is a complex titanium piece heated by two radiant panels placed in a furnace. The AROMM method reduces by a factor 100 the computation time needed to obtain the solution, while keeping an average error below 0.1%. These very good performances open the way for control or identification procedure in a reasonable time for these kind of applications.

Keywords: `Reduced model, modal reduction, finite elements, radiosity, thermal radiation, industrial furnace`

∗. Corresponding author. Tel. :+33 1 69 47 79 36
Email address: `b.gaume@iut.univ-evry.fr` (B. Gaume)

Preprint submitted to International Journal of Heat and Mass Transfer

1. Introduction

Industrial applications involving thermal phenomena in enclosures are frequently encountered : climatic chambers, honeycomb structures, industrial furnaces, ... For realistic configurations, as none of the three modes of heat transfer can be neglected, the problem is complex and a numerical approach is mandatory.

Numerical resolution of heat conduction problems in solids is carried out using classical numerical methods, such as finite elements. However, for complex geometries needing a fine meshing, the time required to solve the problem can become unbearably long. It is especially true if the model is implied in a control or identification loop. To that end, reduced models have been developed [1] [2]. Reduced modal models correspond to a generalization of the Fourier time space separation method :

$$T\left(M,t\right) \approx \sum_{i=1}^{\widetilde{N}} \widetilde{x}_i\left(t\right)\, \widetilde{V}_i\left(M\right) \,. \tag{1}$$

From the knowledge of the reduced base $\widetilde{V}_i$, the unknowns become the excitation states $\widetilde{x}_i$, and the dimension of the problem might be greatly reduced. Modal methods do not degrade the geometry, and give access to the entire temperature field.

Different methods are based on this principle : the most popular is the proper orthogonal decomposition method (POD) which requires the knowledge of thermal fields from experimental or numerical data [3], [4], [5], [6]. The Modal Identification Method (MIM) directly identifies the modal model without determining modes. It is particularly adapted to inverse problems [7] [8]. Finally, in the Amalgam Reduced Order Modal Model (AROMM) method, a modal base is calculated by solving an eigenvalue problem adapted to the considered physical problem. The reduced model is obtained by reducing the initial base by the amalgam method. Initially developed for linear problems [9] [10], this method has since been extended to nonlinear problems [11] [12].

Numerical modeling for natural convection phenomena in enclosures is more delicate, since the entire volume of the cavity is meshed. The grid is refined near the walls to properly capture the dynamics in the boundary layers, leading to a significant increase of the number of degrees of freedom. To limit this number, the simplest solution is to only simulate the solid parts. The internal fluid is then simply modeled by a single temperature and it exchanges a convective heat flux with the walls via a convective coefficient, which is either known from correlations or experimentally. A more sophisticated solution is to employ reduced modal models [13] to simulate the fluid flow. They indeed capture the main characteristics of the flow while highly decreasing the computational complexity.

The addition of radiative phenomena exacerbates the difficulty. The heat radiation is indeed characterized by its spectral dependence, its integration into space, as well as its strong nonlinearity in temperature. When the temperature differences are small, the radiation is modeled by a linearized global coefficient [14]. For simple configurations, analytic relations that express the radiative fluxes

exchanged between surfaces might be used [15]. Otherwise, numerical techniques adapted to heat radiation have been developed. The radiosity method is the reference for gray and diffuse surfaces. First studies focused on very simple geometries : the view factors remain easy to calculate and the number of degrees of freedom is low. For simple cavities, both convection in the fluid and heat radiation between the surfaces were considered [16]. In other works the phenomenon of conduction in the walls has been added [17] [18]. In the 1980s, finite element formulations specific to radiation problems have been developed [19] [20] [21]. In particular, high order finite elements were used for the calculation of radiative fluxes [22] [23]. Other methods exist : Recently the Control Volume - Lattice Boltzmann Method has been introduced by [24], and ANSYS® proposes a specific radiation module using a Hybrid Finite Element Boundary Integral Method [25].

The development of these powerful tools has paved the way to design issues involving radiative transfer. The objective of design is to find the value of a physical quantity that optimizes a process. This is mostly done by iterative procedures which integrate the above mentioned methods. As an example, [26] presents a technique to find the best distribution of heating sources in an oven, in order to obtain the temperature of the heated object as homogeneous as possible. Other functions can be minimized, such as finding the lowest possible wall temperature [27]. As in conduction or convection problems, reduced models could be employed to decrease the computation time needed to solve these optimization processes. As the access to the whole temperature field is imperative for the resolution of radiative dominated problems, modal reduction techniques are appropriate. However, to date, we have not found any study using modal reduction for radiation problems. This article presents an adaptation of the Amalgam Reduced Order Modal Model (AROMM) method for heat radiation and conduction problems in an enclosure.

The paper is structured as follows. In Section 2, the physical description of the considered problem is presented, with a classical finite element formulation. Section 3 investigates the reduced method allowing to solve this problem. Section 4 is dedicated to results and discussion about reduced model. Section 5 offers a conclusion to the paper.

2. Resolution by the finite element method of a thermal problem in an enclosure

2.1. Physical problem

A titanium object with a complex shape is placed on a stand in an industrial furnace. This object is heated by two radiant tubes surrounded by parabolic reflectors located at the top of the furnace (see Fig. 1). The different thermophysical properties of these elements are given in Table 1.

The purpose of this study is to compute the temperature distribution in the titanium object for several exterior boundary conditions and different radiant tubes temperatures. For each scenario, we assume that :

— the furnace exchanges heat with the outside. This is modeled by an equivalent global exchange coefficient h_{ext}. The outside temperature is supposed to be constant at $T_{ext} =$

	Heat capacity $c\,[J.m^{-3}.K^{-1}]$	Thermal conductivity $k\,[W.m^{-1}.K^{-1}]$	Emissivity ε	Thickness $e\,[m]$
Piece	2.35×10^6	21.9	0.8	0.001
Stand	3.95×10^6	16.3	0.95	0.005
Wall	0.18×10^6	45	0.95	0.01
Tube	3.4×10^6	45	0.95	0.01
Reflector	3.95×10^6	16.3	0.3	0.001

TABLE 1: Thermophysical characteristics of the different components

$293.15K$;

— the convective exchanges between the interior surfaces of the furnace are represented by a constant coefficient $h_{int} = 5\,W.m^{-2}.K^{-1}$;

— the radiant tubes are considered to be at constant temperature T_{tube}.

Table 2 presents the parameter values for the different scenarios.

	$h_{ext}[W.m^{-2}.K^{-1}]$	$T_{tube}[K]$
Scenario 1	5	673.15
Scenario 2	1	973.15
Scenario 3	0.5	1273.15

TABLE 2: Variable boundary conditions

The initial condition is the ambiant temperature $T_0 = 293.15K$, and the simulation duration to reach the steady state is $5 \times 10^4\,s$. Considering the high temperature of the tubes, the heating of the titanium piece is mainly driven by radiative transfer. The complex geometry creates masks, and a fine detailed resolution of the radiative flux is mandatory to correctly represent the temperature evolution.

2.2. Finite element formulation of the problem

2.2.1. Adaptating the heat equation for thin shells in an enclosure

Considering the above characteristics, the maximum Biot Number is $Bi = \dfrac{h\,e}{2\,k} \leq 0.072$ (with $e = 0.5\,cm$, $k = 16.3\,W.m^{-1}.K^{-1}$ and $h_{max} = 4\varepsilon\sigma T_{max}^3 \simeq 500\,W.m^{-2}.K^{-1}$), validating a shell model hypothesis [28] [29]. In a shell model, the temperature field depends only on local coordinates (η, ζ) of a plane Ω, which corresponds to the main surface of the original 3D domain (see Fig. 2). Both faces $\Omega_{(+)}$ and $\Omega_{(-)}$, characterized by normal vectors of opposite signs (Fig. 3.a), receive a heat flux

φ. The weak formulation of the heat equation yields :

$$\int_{\Omega} e\,c\frac{\partial T}{\partial t} f\,d\Omega = -\int_{\Omega} e\,k\,\vec{\nabla}T\cdot\vec{\nabla}f\,d\Omega + \int_{\Omega_{(+)}} \varphi\,f\,d\Omega + \int_{\Omega_{(-)}} \varphi\,f\,d\Omega\,, \tag{2}$$

where $f \in H_1(\Omega)$ ($H_1(\Omega)$ being the Hilbert space such that f and its derivatives are square-integrable functions) is the test function of the variational formulation on Ω.

Faces $\Omega_{(+)}$ and $\Omega_{(-)}$ can be rearranged based on their location, outside or inside the enclosure (Fig. 3.b).

For external surfaces Ω_{ext}, a simple global exchange coefficient models furnace insulation :

$$\int_{\Omega_{ext}} \varphi\,f\,d\Omega = \int_{\Omega_{ext}} h_{ext}\,(T_{ext} - T)\,f\,d\Omega\,. \tag{3}$$

For interior surfaces Ω_{int}, the heat flux is divided into distinct convective and radiative phenomena :

$$\int_{\Omega_{int}} \varphi\,f\,d\Omega = \int_{\Omega_{int}} h_{int}\,\left(T_{int}\,(T) - T\right)\,f\,d\Omega + \int_{\Omega_{int}} \varphi_{rad}\,f\,d\Omega\,, \tag{4}$$

where $T_{int}(T)$ is the unique air temperature inside the furnace. Assuming that the heat capacity of the internal fluid is negligible compared to that of the walls, a simple heat balance provides the expression of indoor temperature :

$$T_{int}\,(T) = \frac{\int_{\Omega_{int}} h_{int}\,T d\Omega}{\int_{\Omega_{int}} h_{int}\,d\Omega}\,. \tag{5}$$

Equation (2) finally becomes :

$$\begin{aligned}\int_{\Omega} e\,c\frac{\partial T}{\partial t} f\,d\Omega = &-\int_{\Omega} e\,k\,\vec{\nabla}T\cdot\vec{\nabla}f\,d\Omega \\ &-\int_{\Omega_{int}} h_{int}\,T\,f\,d\Omega + \int_{\Omega_{int}} h_{int}\,T_{int}\,(T)\,f\,d\Omega \\ &-\int_{\Omega_{ext}} h_{ext}\,T\,f\,d\Omega + \int_{\Omega_{ext}} h_{ext}\,T_{ext}\,f\,d\Omega \\ &+\int_{\Omega_{int}} \varphi_{rad}\,f\,d\Omega\,,\end{aligned} \tag{6}$$

where T_{int} is defined by relation (5).

2.2.2. Modeling the radiative heat flux with the radiosity method

In this problem, diffuse-gray bodies exchanging radiative heat flux are placed in a nonparticipating media. The radiative heat flux exchanged by a surface depends, in a complex way, on the temperature distribution of the surrounding surfaces. This flux can be obtained by the net-radiation method [17] [30]. The considered surface is first discretized in N_p elementary surfaces Ω_j^e, on which the radiative flux is considered constant, $\varphi_{rad} = \overline{\varphi}_j$. These elementary surfaces are named 'patches'.

The ${N_p}^2$ view factors F_{ij}, which are the proportion of flux leaving a patch Ω_i^e towards another elementary surface Ω_j^e, are then computed with the polar-plane-based method [31] [32], which is an adaptation of the hemicube method [33]. An hemisphere centered on Ω_i^e (Fig. 4) is discretized in N^q quadrangles. Their size is defined so that the value of the elementary view factors towards Ω_j^e is constant. This avoids to compute and keep track of the elementary view factors. The hemisphere is then projected on a plan parallel to Ω_i^e. Surface Ω_j^e is finally projected on this plan. The view factor is retrieved from the sum of the quadrangles covered by this projection.

The radiosity method relates the mean flux $\overline{\varphi}_i$ exchanged by patch Ω_i^e to the set of mean temperatures $\overline{T}_j$, with $j \in [1, N_p]$:

$$\forall j \in [1, N_p] \quad \sum_{i=1}^{N_p} \left[\frac{\delta_{ji}}{\varepsilon_i} - \left(\frac{1}{\varepsilon_i} - 1 \right) F_{ji} \right] \overline{\varphi}_i = - \sum_{i=1}^{N_p} \left(\delta_{ji} - F_{ji} \right) \sigma \overline{T}_i^4 \,, \tag{7}$$

where δ_{ji} is the Kronecker delta. This sign convention ensures that exchanged flux $\overline{\varphi}_i$ is negative if the surface S_i emits more flux than it absorbs. Relation (7) can be written in matrix form :

$$\mathbf{A}\,\overline{\varphi} = \mathbf{B}\,\overline{\mathbf{T}}^{\mathbf{4}} \,. \tag{8}$$

The mean flux exchanged by a patch $\overline{\varphi}_j$ expresses as :

$$\overline{\varphi}_j = \sum_{i=1}^{N_p} r_{ji} \overline{T}_i^4 \,, \tag{9}$$

where r_{ji} are the elements of $\mathbf{R}_{rad}\,[N_p,\, N_p] = \mathbf{A}^{-1}\,\mathbf{B}$.

2.2.3. Variational formulation with radiative heat flux

The variational expression of the exchanged radiative flux is derived from Eqs. (4) and (9) :

$$\begin{aligned}\int_{\Omega_{int}} \varphi_{rad}\, f\, d\Omega &= \sum_{j=1}^{N_p} \int_{\Omega_j^e} \varphi_{rad}\, f\, d\Omega \\ &= \sum_{j=1}^{N_p} \overline{\varphi}_j \int_{\Omega_j^e} f\, d\Omega \\ &= \sum_{j=1}^{N_p} \sum_{i=1}^{N_p} \left(r_{ji} \overline{T}_i^4\right) \int_{\Omega_j^e} f\, d\Omega\,.\end{aligned} \tag{10}$$

115 The addition of this term to the variational formulation Eq. (6) leads to :

$$\begin{aligned}\int_{\Omega} e\, c \frac{\partial T}{\partial t} f\, d\Omega = &- \int_{\Omega} e\, k\, \vec{\nabla} T \cdot \vec{\nabla} f\, d\Omega \\ &- \int_{\Omega_{int}} h_{int} T\, f\, d\Omega - \int_{\Omega_{ext}} h_{ext}\, T\, f\, d\Omega \\ &+ \int_{\Omega_{int}} h_{int}\, T_{int}\, f\, d\Omega + \int_{\Omega_{ext}} h_{ext}\, T_{ext}\, f\, d\Omega \\ &+ \sum_{j=1}^{N_p} \sum_{i=1}^{N_p} \left(r_{ji} \overline{T}_i^4\right) \int_{\Omega_j^e} f\, d\Omega\,.\end{aligned} \tag{11}$$

2.3. Numerical resolution

The spatial discretization of the problem defined by Eqs. (5) and (11) through Lagrange finite elements brings out the following matrix problem (hereafter called detailed model) :

$$\mathbf{C} \frac{d\mathbf{T}}{dt} = \left[\mathbf{K} + \mathbf{H_{int}} + \mathbf{H_{ext}}\right] \mathbf{T} + \mathbf{U_{cpl}}\, T_{int}\left(\mathbf{T}\right) + \mathbf{U_0} + \overline{\mathbf{R}}_{rad} \overline{\mathbf{T}}^4\,. \tag{12}$$

Vector $\mathbf{T}$ contains the temperature value at the N discretization points, and $\mathbf{U_0}$ is a vector representing the external known solicitations (the received external heat flux $\int_\Omega h_{ext} T_{ext}$). $\mathbf{C}$, $\mathbf{K}$, $\mathbf{H_{int}}$, $\mathbf{H_{ext}}$ are $[N \times N]$ symmetric sparse matrices : $\mathbf{C}$ is the thermal inertia matrix, $\mathbf{K}$ the conductivity matrix and $\mathbf{H_{int}}$ and $\mathbf{H_{ext}}$ are accommodation matrices. Vector $\mathbf{U_{cpl}}$ represents the convective

	N_t	N_p	$(< S_{\Omega_i^e} >)\ (m^2)$
Piece	2 891	5 782	5.02×10^{-4}
Stand	1 562	3 124	1.15×10^{-3}
Wall	3 566	3 566	2.80×10^{-3}
Tubes	11 144	22 288	3.90×10^{-5}
Reflectors	5 039	10 078	2.60×10^{-3}
Total	24 202	44 838	

TABLE 3: Number of triangular elements (N_t) and number of patches (N_p) of the different components

exchange with the air inside the furnace, at temperature $T_{int}(\mathbf{T})$. This latter term is computed thanks to the discretization of Eq. (5) :

$$T_{int}(\mathbf{T}) = \mathbf{D}\,\mathbf{T}\,. \tag{13}$$

Vector $\overline{\mathbf{T}}$ of dimension $[N_p]$ contains mean temperatures of every patch Ω_i^e and is easily estimated by :

$$\overline{\mathbf{T}} = \mathbf{U_R}\,\mathbf{T}\,. \tag{14}$$

Matrix $\mathbf{U_R}$ of dimension $[N_p \times N]$ is the average operator which allows to computes the mean temperature on the N_p patches from the temperature at the N nodes of the mesh.
Finally, radiation matrix $\overline{\mathbf{R}}_{rad}$ $[N \times N_p]$ allots the mean heat flux density from the N_p patches to the N nodes. This matrix is computed with the following relation

$$\overline{\mathbf{R}}_{rad} = (\mathbf{U_R})^T\,\mathbf{S}\,\mathbf{R}_{rad}\,,$$

where $\mathbf{S}$ is a diagonal matrix of dimension $[N_p \times N_p]$ such that S_{ii} contains the surface of the patch i. The components of vector $\overline{\mathbf{T}}^4$ contains the components of the vector $\overline{\mathbf{T}}$ to the power 4.

2.4. Results

All calculations were performed on a laptop with a 6-core Intel® Xeon® E-2176M @ 2.7GHz and 64GB of RAM. The discretization used for all the calculations is a meshing of $N = 12\,167$ nodes which define $N_t = 24\,202$ triangular elements. Table 3 details the meshing component by component. The mesh has only been refined on the radiant tubes, the source of luminance, so that the direction of the emitted flux is well defined, and also on the platinum object, which is the critical parameter. The determination of the patches is an open question. In this study, the patches coincide with the triangles of the mesh. As inner surfaces are doubled (they radiate via their two faces $\Omega_{(+)}$ and $\Omega_{(-)}$, see Fig. 3), $N_p = 44\,838$ patches Ω_j^e emerge. First step is to perform the preliminary calculation needed by radiation. The computation time needed to get the ${N_p}^2$ view factors is $t_{CPU}^{F_{ij}} \approx 1h$. The computation of $\mathbf{A}^{-1}\mathbf{B}$ lasts $t_{CPU}^{rad} \approx 8h$. These two calculations are performed only once and are therefore reused for each simulation.

The temporal discretization of equation (12) is done with a semi-implicit second-order scheme with variable time steps [34].

The numerical simulation of $5 \times 10^4\, s$ requires a CPU time that is dependent on nonlinearities, as it varies between 4 and 6 hours.

Figure 5 presents temperature fields at $t = 3\,000\, s$ for the three scenarios, characterized by very different heat source temperature. The first remark concerns the temperature range. As the maximum temperature goes from $673.15\, K$ to $973.15\, K$ (scenario 1 and 2), the minimum temperature increases only of $55\, K$. But when another increase of $300\, K$ is applied on the radiant tubes temperature (scenario 3), minimum temperature gains more than $150\, K$, underlining the non-linear effect of radiation. The second remark concerns the shape of the temperature fields. As the heat transfer by radiation is predominant, mask effect plays a significant role. This is particularly apparent on the titanium object. For scenario 3, its top surface is at almost $800\, K$, while the bottom one, which is not directly exposed to the radiant tubes, is around $600\, K$. Finally, even if the temperature contour on the titanium item barely changes from one simulation to another, its temperature amplitude is obviously dependent on the applied scenario. This preliminary study shows that the radiation has to be modeled in all its complexity to give significant results. This fine modeling results in an important CPU time, which forbids parametric study, hence the need for reduced models considering radiation.

3. Modal method

In modal methods, the temperature field $T(M,t)$ is searched as a weighted sum of elementary functions V_i called modes :

$$T(M,t) = \sum_{i=1}^{\infty} x_i(t)\ V_i(M)\,. \tag{15}$$

Weighting coefficients $x_i(t)$ are now the unknowns, called excitation states. Virtually, the sum does not reach infinity. When the modes are obtained after spatial discretization, the number of modes numerically accessible corresponds to the number of mesh points N.

Different modal approaches exist. In this study, modes are eigenfunctions of the Laplace operator, with Neumann Boundary conditions :

$$-\int_\Omega e\,k\,\vec{\nabla}V_i\cdot\vec{\nabla}f\,d\Omega = z_i\int_\Omega e\,c\,V_i\,f\,d\Omega\,, \tag{16}$$

where z_i is the associated eigenvalue, homogeneous to the inverse of a time.

Orthogonality relationships play a fundamental role in modal methods. They ensure that the decomposition (15) is unique. Modes defined by Eq. (16) verify the following relations :

$$\forall i,j\in[1,N]\,,\qquad \int_\Omega e\,c\,V_i\,V_j\,d\Omega = \delta_{ij}, \tag{17}$$

$$\forall i,j\in[1,N]\,,\qquad \int_\Omega e\,k\,\vec{\nabla}V_i\cdot\vec{\nabla}V_j\,d\Omega = z_i\,\delta_{ij}. \tag{18}$$

3.1. Reduction step

The purpose of the modal reduction is to approach the thermal field with a reduced base $\left(\widetilde{z}_i, \widetilde{V}_i\right)$, of dimension $\widetilde{N} << N$:

$$\tilde{T}(M,t) = \sum_{i=1}^{\tilde{N}} \widetilde{x}_i(t)\ \widetilde{V}_i(M)\,. \tag{19}$$

This is performed by the amalgam reduction method. In this method, dominant modes are selected. The remaining modes, called minors, are aggregated to the dominant ones, instead of being discarded. The resulting reduced modes, named amalgamated modes, are then a linear combination of the original modes :

$$\forall i \in \left\{1, ...\tilde{N}\right\}\ \ \widetilde{V}_i(M) = V_{i,0} + \sum_{p=1}^{N_i} \alpha_{i_p} V_{i_p}\,. \tag{20}$$

The specificity of the amalgam method is to keep every mode of the original base. To ensure the orthogonality of the reduced basis, each original eigenvector V_i is used only once. The distribution of the original modes V_i in the reduced basis $\widetilde{V}_i$, and the determination of the weighting coefficient α_{i_p} are obtained by minimizing in the modal space an energy difference on a reference simulation (more details can be found in [11]). The reference simulation shall trigger the relevant modes, and should be readily computed. In the case of a radiative problem, all surfaces are considered as black-bodies in the reference simulation. The computation is greatly simplified, as $\mathbf{A}$ becomes the identity matrix in Eq. (8).

3.2. Modal formulation of the problem

3.2.1. Reduced formulation

The modal formulation is obtained by replacing temperature by its decomposition on the Neumann modes in Eq. (11). Neumann modes are also used for test functions f. The following equation

is obtained :

$$
\begin{aligned}
\sum_{p=1}^{\widetilde{N}} \int_{\Omega} e\, c \widetilde{V}_p\, \widetilde{V}_q\, d\Omega\, \frac{\partial \widetilde{x}_p}{\partial t} = & - \sum_{p=1}^{\widetilde{N}} \int_{\Omega} e\, k\, \vec{\nabla} \widetilde{V}_p \cdot\, \vec{\nabla} \widetilde{V}_q\; d\Omega\, \widetilde{x}_p \\
& - \sum_{p=1}^{\widetilde{N}} \left(\int_{\Omega_{int}} h_{int} \widetilde{V}_p\, \widetilde{V}_q\, d\Omega + \int_{\Omega_{ext}} h_{ext} \widetilde{V}_p\, \widetilde{V}_q\, d\Omega \right) \widetilde{x}_p \\
& + \sum_{p=1}^{\widetilde{N}} \left(\int_{\Omega_{int}} h_{int}\, T_{int}\, \widetilde{V}_q\, d\Omega + \int_{\Omega_{ext}} h_{ext}\, T_{ext}\, \widetilde{V}_q\, d\Omega \right) \\
& + \sum_{p=1}^{\widetilde{N}} \sum_{j=1}^{N_p} \sum_{i=1}^{N_p} \left(r_{ji} \overline{T}_i^4 \right) \int_{\Omega_j^e} \widetilde{V}_q\, d\Omega\,.
\end{aligned}
\tag{21}
$$

The temperature of the air inside the enclosure, as well as $\overline{T}_i$, the mean temperature on the patch Ω_i^e, can also be expressed under a modal formulation :

$$
T_{int} = \frac{\sum_{i=1}^{\widetilde{N}} x_i \int_{\Omega_{int}} h_{int}\, \tilde{V}_i d\Omega}{\int_{\Omega_{int}} h_{int}\, d\Omega} \quad , \quad \overline{T}_i = \frac{\sum_{j=1}^{\widetilde{N}} x_j \int_{\Omega_i^e} \tilde{V}_j d\Omega}{\int_{\Omega_i^e} d\Omega}\,. \tag{22}
$$

The modal formulation of T_{int} in Eq. (22) is injected in Eq. (21). However, as $\overline{T}_i^4 \neq \overline{T_i^4}$, it can not be done for $\overline{T}_i$. The repeated change of basis between modal and temperature space will deteriorate the expected gain in computation time.

3.3. Numerical resolution

The set of equations (21) and (22) can be written under matrix form :

$$
\widetilde{\mathbf{V}}^T\, \mathbf{C}\, \widetilde{\mathbf{V}} \frac{d\widetilde{\mathbf{X}}}{dt} = \widetilde{\mathbf{V}}^T \left[\mathbf{K} + \mathbf{H_{int}} + \mathbf{H_{ext}} + \mathbf{H_{cpl}} \right] \widetilde{\mathbf{V}} \widetilde{\mathbf{X}} + \widetilde{\mathbf{V}}^T \mathbf{U_0} + \widetilde{\mathbf{V}}^T\, \overline{\mathbf{R}}_{rad}\, \overline{\mathbf{T}}^4\,, \tag{23}
$$

with

$$
\overline{\mathbf{T}} = \mathbf{U_R}\, \widetilde{\mathbf{V}}\, \widetilde{\mathbf{X}}\,, \tag{24}
$$

where $\widetilde{\mathbf{V}} \left[\widetilde{N} \times \widetilde{N} \right]$ is the matrix containing the $\widetilde{N}$ discrete reduced modes $\widetilde{V}_p$, and $\mathbf{C}$, $\mathbf{K}$, etc. are finite element matrices defined in Eq. (12). Compact matrices like $\widetilde{\mathbf{V}}^T\, \mathbf{C}\, \widetilde{\mathbf{V}}$ are dense and of dimension $\left[\widetilde{N} \times \widetilde{N} \right]$.

4. Results and discussion

4.1. Reduced model creation

The creation of the reduced model demands preliminary computations. As for the finite element model, view factors have to be computed, and the inversion of matrix $\mathbf{A}$ in Eq. (8) has to be performed. This is done in 9 hours. The second step consists in the computation of the modal base (Eq. (16)), done in 4 minutes. Figure 6 depicts typical examples of Neumann eigenmodes. They can be seen as temperature fields, solution of the steady-state heat equation where the volume solicitation is proportional to the temperature. For homogeneous domain, these eigenmodes are basically a combination of trigonometric functions. As the order of the eigenmodes increases, its time constant decreases, yielding modes that vanish quickly. This occurs with an increase of the spatial frequency, as, for instance, shown by mode 599. Typically, with a simple truncation reduction procedure, this mode will be discarded, together with the spatial information it contains. With the amalgam procedure, this mode is kept, but its time behaviour will be imposed by another mode.

The amalgam procedure requires a reference field. As stated above, this reference field is obtained by a finite element simulation with all surfaces considered as black bodies. By doing so, the numerical problem is greatly simplified. Moreover, the reference simulation is performed over a very short period of $1\,800s$ instead of $50\,000s$. With these two simplifications, the reference simulation is done in about 2 minutes. The amalgam procedure in itself is performed in ten seconds. Figure 7 shows amalgamated modes. From the Neumann eigenmodes, the amalgam procedure built new modes related to the solicitations. This is evidenced by mode 3, where the temperature contour on the titanium object is similar to those shown in Fig. 5, while mode 12 provides a contribution to the parabolic reflectors.

4.2. Reduced Model utilization

Figure 8 illustrates the performance of AROMM method in terms of accuracy. The modal temperature field computed with a reduced model of order 200 (compared to the 12 167 nodes of the original model) is represented for scenario 3 at $t = 3000\,s$, and should be confronted to Fig. 5 (c) (same scale and contours are used). Visually the agreement between these two fields is excellent. In particular, contours produced by the complex radiative heat transfer are remarkably well recovered. This is confirmed by the difference field $|T - \tilde{T}|$ represented in the same figure. This field is erratic, which is characteristic of modal reduction. The difference does not exceed $26\,K$, which has to be related to the $1\,200\,K$ of radiant tubes. The average difference of $3.3\,K$ (which represents 0.2% of $1200\,K$) is very satisfactory. Note also that the maximum temperature reached by the titanium piece is particularly well predicted by the modal model with a difference of prediction with the finite element model of less than $1.5\,K$.

A sensitivity analysis on the reduction order has been conducted. To quantify its results the

following quantities are defined :

$$< \varepsilon >= \frac{1}{V}\frac{1}{\tau}\frac{\int_\tau \int_\Omega |T-\tilde{T}| d\Omega}{\max\limits_{\tau,\Omega}(T) - \min\limits_{\tau,\Omega}(T)} \quad , \quad \varepsilon_{max} = \frac{\max\limits_{\tau,\Omega}|T-\tilde{T}|}{\max\limits_{\tau,\Omega}(T) - \min\limits_{\tau,\Omega}(T)},$$

where τ is the simulation duration and V the volume of domain Ω.

The main conclusions are summarized in Fig. 9. Figure 9 (a) represents $< \varepsilon >$ and ε_{max} as a function of the order of the modal model for the three scenarios. The CPU time required to solve the problem is also represented in Fig. 9 (b). For the three scenarios, even for highly reduced model (20 modes), results are decent, with $\varepsilon_{max} \approx 10\%$ and $< \varepsilon >$ below 1%. However, despite those very good relative errors, the absolute errors are less satisfying : for scenario 3, the maximum error with a reduced model of order 20 reaches $100\,K$. Still, about an order of magnitude is found between the maximum and mean errors : the maximum error is localized in both time and space. Obviously, errors decrease monotonously as the model order increases. With 200 modes, $< \varepsilon >$ is below 0.1% ($\approx 1\,K$) while ε_{max} is under 3%. The choice of the order is a question of compromise between accuracy and computation time. The latter logically increases with the order of the model. It still remains very small compared to the computation time required for the resolution by classical finite element model (several hours). With a reduced model of order 200, CPU time for scenario 3 is 4 minutes, which is almost a hundred time faster than the FE model which requires 6 hours. As the reduced model has proven its efficiency on three scenarios characterized by different thermal solicitations (different global exchange coefficients and different radiant tube temperature), it is suitable for parametric study, or control loops.

5. Conclusion

The purpose of this study was to demonstrate the feasibility and the relevance of reducing a thermal radiation problem for a realistic configuration, while keeping the complexity engendered by the radiation and the geometry. The employed method combines a modal reduction technique and the radiosity method. Indeed, modal methods give access to the whole temperature field, which is mandatory in radiative dominated problems. In this study, we used a Neumann base reduced by the amalgam method. The computation of the modal model in itself is effortless (less than 7 minutes). However, some computations required by the radiosity method could not be avoided, such as the view factors determination or the inversion of the radiosity matrix. The overall entrance ticket for using a modal model with an accurately modeled radiation might seem expensive, as it requires nine hours of computation. However, this time has to be compared to a finite elements simulation which can demand up to six hours of CPU time.

To be relevant to other methods, the resulting reduced model has to be used several times and not computed for a one-shot study. The modal reduced model has proven to be robust, as three different configurations were tested, each having different boundary conditions and different radiative solicitations. With a modal model of order 200, the relative maximal error was found to be less

than 3% while the average error in time and space is below 0.1%. At that order, the computation effort is very low, as only 4 minutes are needed to solve a duration of $50\,000\,s$, compared to the 6 hours required by the finite elements problem. The gain in computation time is of the order of 100 or more, whatever the configuration tested. These very satisfying performances open access to real time control or identification procedure with radiation.

Références

[1] S. Carmona, Y. Rouizi, O. Quéméner, F. Joly, A. Neveu, Estimation of heat flux by using reduced model and the adjoint method. application to a brake disc rotating, International Journal of Thermal Sciences 131 (2018) 94 – 104. doi:https://doi.org/10.1016/j.ijthermalsci.2018.04.036.
URL http://www.sciencedirect.com/science/article/pii/S1290072917311171

[2] S. Carmona, Y. Rouizi, O. Quéméner, Spatio-temporal identification of heat flux density using reduced models. application to a brake pad, International Journal of Heat and Mass Transfer 128 (2019) 1048 – 1063. doi:https://doi.org/10.1016/j.ijheatmasstransfer.2018.09.043.
URL http://www.sciencedirect.com/science/article/pii/S001793101831785X

[3] J. A. Atwell, B. B. King, Proper orthogonal decomposition for reduced basis feedback controllers for parabolic equations, Mathematical and Computer Modelling 33 (2001) 1–19.

[4] X. Zhang, H. Xiang, A fast meshless method based on proper orthogonal decomposition for the transient heat conduction problems, Int. J. Heat Mass Transfer 84 (2015) 729 – 739.

[5] R. Ghosh, Y. Joshi, Error estimation in POD-based dynamic reduced-order thermal modeling of data centers, Int. J. Heat Mass Transfer 57 (2013) 698 – 707.

[6] X. He, Q. Kong, Z. Xiao, Fast simulation methods for dynamic heat transfer through building envelope based on model-order-reduction, in : P. Engineering (Ed.), 9th International Symposium on Heating, Ventilation and Air Conditioning (ISHVAC) and the 3rd International Conference on Building Energy and Environment (COBEE), Vol. 121, 2015, pp. 1764–1771.

[7] Y. Rouizi, Y. Favennec, Y. Jarny, D. Petit, Model reduction through identification - Application to some diffusion - convection problems in heat transfer, with an extension towards control strategies, C.R. Mec. 341 (2013) 776 – 792.

[8] E. Videcoq, M. Girault, K. Bouderbala, H. Nouira, J. Salgado, D. Petit, Parametric investigation of linear quadratic gaussian and model predictive control approaches for thermal regulation of a high precision geometric measurement machine, Appl. Therm. Eng. 78 (2015) 720 – 730.

[9] J. Sicard, P. Bacot, A. Neveu, Analyse modale des échanges thermiques dans le bâtiment, Int. J. Heat Mass Transfer 28 (1985) 111–123.

[10] Y. Gao, J. Roux, C. Teodosiu, L. Zhaoa, Reduced linear state model of hollow blocks walls, validation using hot box measurements, Energy and Buildings 36 (2004) 1107–1115.

[11] O. Quéméner, A. Neveu, E. Videcoq, A specific reduction method for branch modal formulation : Application to highly non linear configuration, Int. J. Thermal Sci. 46 (9) (2006) 890–907.

[12] E. Videcoq, M. Lazard, O. Quéméner, A. Neveu, Online temperature prediction using a branch eigenmode reduced model applied to cutting process, Numerical Heat Transfer, Part A 55 (2009) 683–705.

[13] A. Tallet, C. Allery, F. Allard, Pod approach to determine in real-time the temperature distribution in a cavity, Building and Environment 93 (2015) 34 – 49. doi:https://doi.org/10.1016/j.buildenv.2015.07.007.
URL http://www.sciencedirect.com/science/article/pii/S036013231530055X

[14] V. Harish, A. Kumar, Reduced order modeling and parameter identification of a building energy system model through an optimization routine, Appl. Energy 162 (2016) 1010 – 1023.

[15] S. Yoo, Y. Kim, S. Kim, N. Jung, D. Im, J. Gong, J. Lee, K. Park, Y. Oh, Verification of radiation heat transfer analysis in kstar pfc and vacuum vessel during baking, Fusion Engineering and Design 109-111 (PA) (2016) 73–77.

[16] M. Bouafia, S. Hamimid, M. Guellal, Non-boussinesq convection in a square cavity with surface thermal radiation, International Journal of Thermal Sciences 96 (2015) 236–247.

[17] T. Ait-taleb, A. Abdelbaki, Z. Zrikem, Numerical simulation of coupled heat transfers by conduction, natural convection and radiation in hollow structures heated from below or above, Int. J. Therm. Sci. 47 (2008) 378 – 387.

[18] M. A. Antar, H. Baig, Conjugate conduction-natural convection heat transfer in a hollow building block, Appl. Therm. Eng. 29 (2009) 3716 – 3720.

[19] K.-J. Bathe, M. R. Khoshgoftaar, Finite element formulation and solution of nonlinear heat transfer, Nuclear Engineering and Design 51 (3) (1979) 389 – 401. doi:https://doi.org/10.1016/0029-5493(79)90126-2.
URL http://www.sciencedirect.com/science/article/pii/0029549379901262

[20] P. S. Heckbert, Finite element method for radiosity, 20th SIGGRAPH 1993 Anaheim, CA, USA (1993).

[21] W. Minkowycz, A. Haji-Sheikh, The sparrow galerkin solution of radiation exchange and transition to finite element, International Journal of Heat and Mass Transfer 42 (8) (1999) 1353–1362.

[22] D. C. Gould, Radiation heat transfer between diffuse-gray surfaces using higher order finite elements, 34th AIAA Thermophysics Conference 19-22 June 2000 / Denver, CO (2000).

[23] L. Yi, Y. Peng, Q. Sun, Research of the higher-order finite element arithmetic for radiation exchange, Chinese Journal of Aeronautics 19 (3) (2006) 197–202.

[24] F. Bouzgarrou, F. Askri, H. Belhaj Ali, S. Ben Nasrallah, Analyses of unsteady conduction-radiation heat transfer using unstructured lattice boltzmann method, International Journal of Thermal Sciences 116 (2017) 287–309.

[25] J. Silvestro, Hybrid finite element boundary integral method, ANSYS (2018).
URL https://support.ansys.com/staticassets/ANSYS/staticassets/resourcelibrary/whitepaper/wp-HFSS-Hybrid-Finite-Element-Integral-Equation-Method.pdf

[26] R. P. Chopade, S. C. Mishra, P. Mahanta, S. Maruyama, Estimation of power of heaters in a radiant furnace for uniform thermal conditions on 3-d irregular shaped objects, International Journal of Heat and Mass Transfer 55 (15-16) (2012) 4340–4351.

[27] D. Castro, C. Kiyono, E. Silva, Design of radiative enclosures by using topology optimization, International Journal of Heat and Mass Transfer 88 (2015) 880–890.

[28] A. E. Jeffers, Heat transfer element for modeling the thermal response of non-uniformly heated plates, Finite Elements in Analysis and Design 63 (2013) 62 – 68.

[29] C. An, J. Su, Lumped models for transient thermal analysis of multilayered composite pipeline with active heating, Appl. Therm. Eng. 87 (2015) 749 – 759.

[30] M. A. Antar, Thermal radiation role in conjugate heat transfer across a multiple-cavity building block, Energy 35 (2010) 3508 – 3516.

[31] J. R. Wallace, M. F. Cohen, D. P. Greenberg, A twopass solution to the rendering equation : a synthesis of ray tracing and radiosity methods, Computer Graphics 21 (4) (1987) 331–320.

[32] Y. Zhou, Q. Peng, The super-plane buffer ; an efficient form-factor evaluation algorithm for progressive radiosity, Comput. & Graphic 16 (2) (1992) 151–158.

[33] M. F. Cohen, D. P. Greenberg, The hemi-cube : A radiosity solution for complex environments, Computer Graphics 19 (3) (1985) 31–40, SIGGRAPHJ'85 Proceedings (July 1985).

[34] D. Wang, Variable step-size implicit-explicit linear multistep methods for time-dependent PDEs, Master's thesis, Department of mathematics, Harbin Institue of Technology (2005).

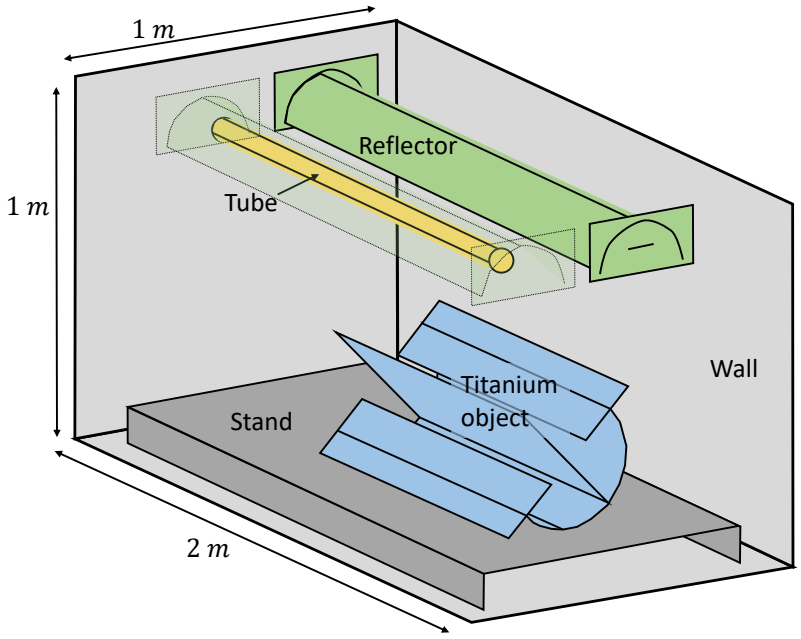

FIGURE 1: The considered geometry

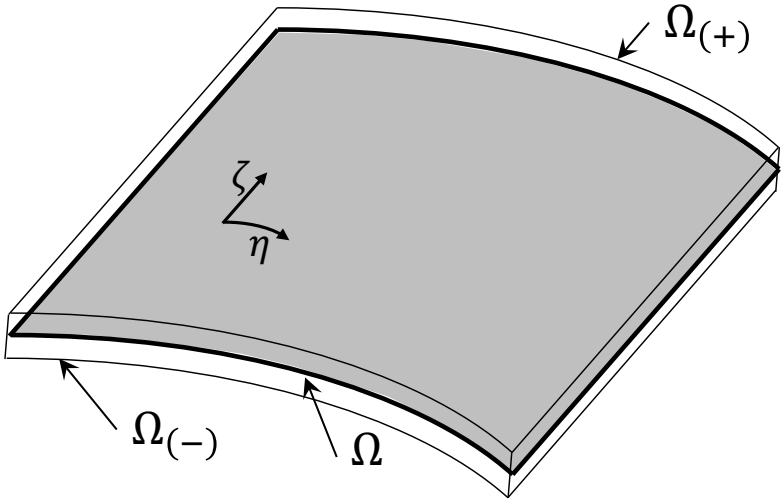

FIGURE 2: Transformation of a 3D domain to a shell configuration

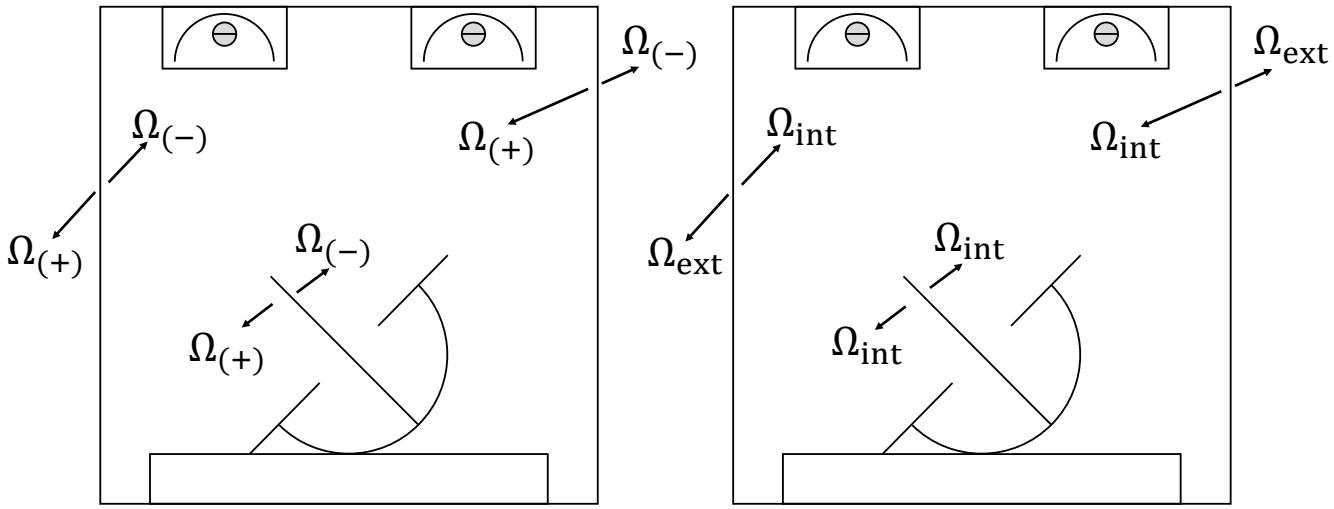

FIGURE 3: Decompositions of boundaries in a shell configuration

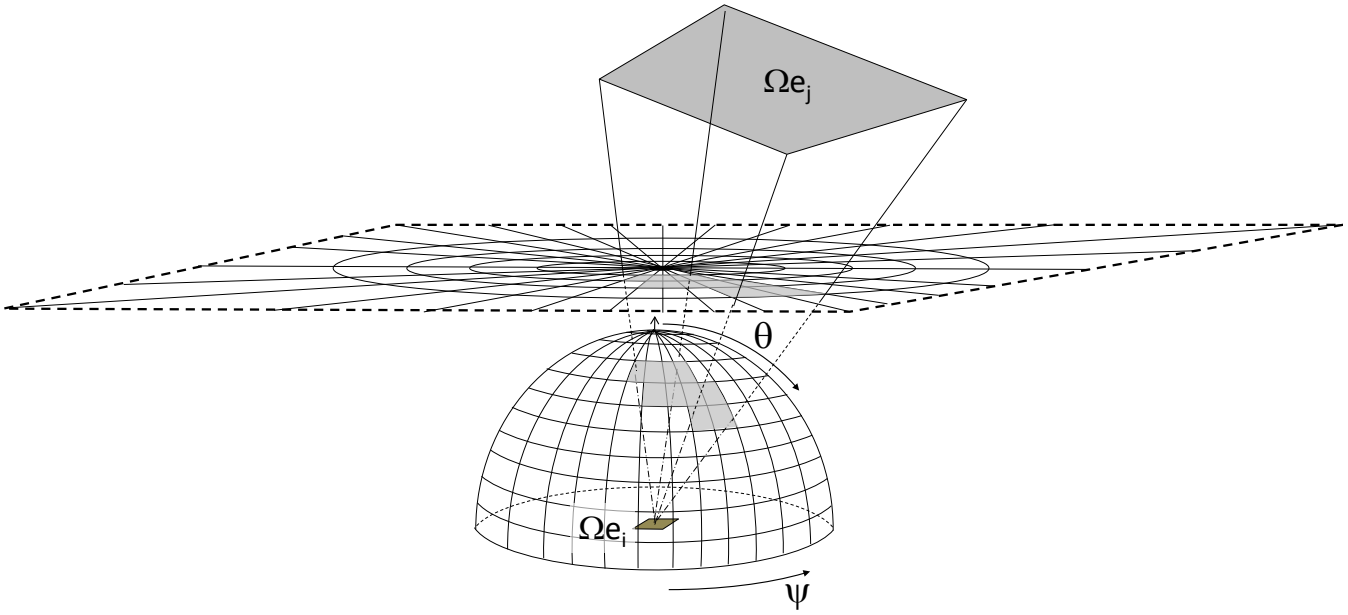

FIGURE 4: Projection using polar-plane-based method

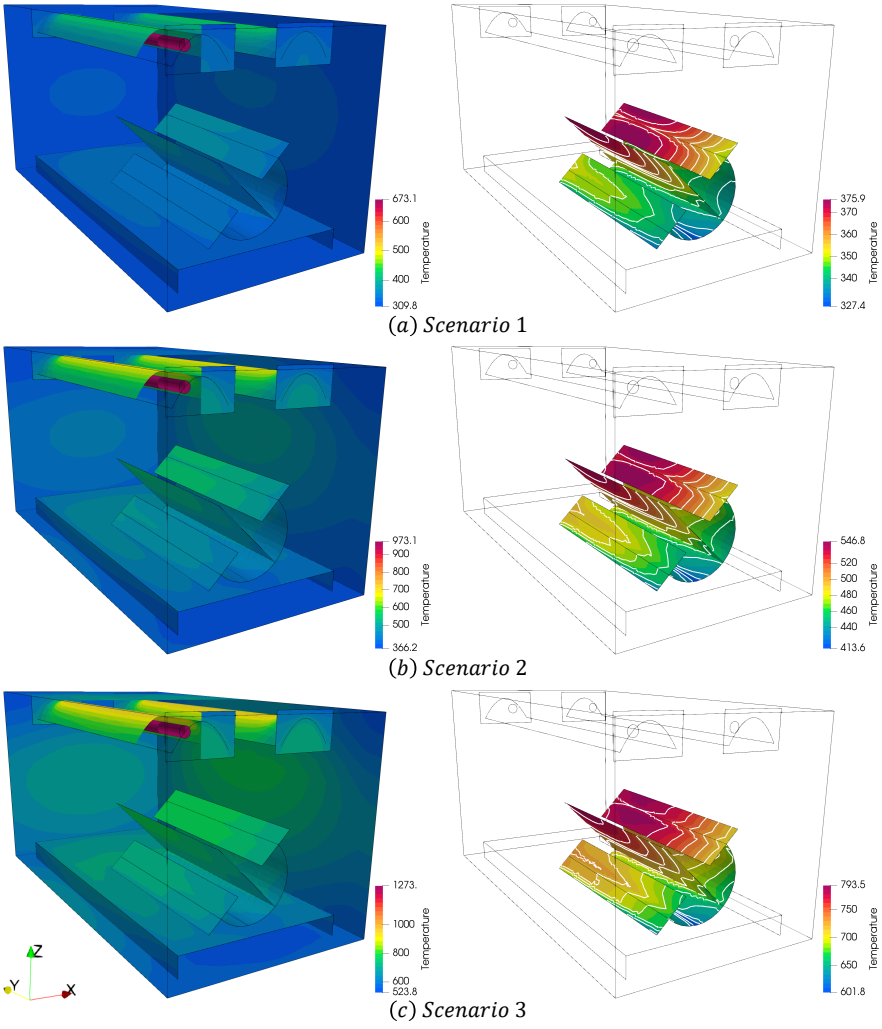

FIGURE 5: Temperature fields for the three scenarios at time 3 000 s. The left column represents the complete thermal scene, whereas the right column focuses on titanium item

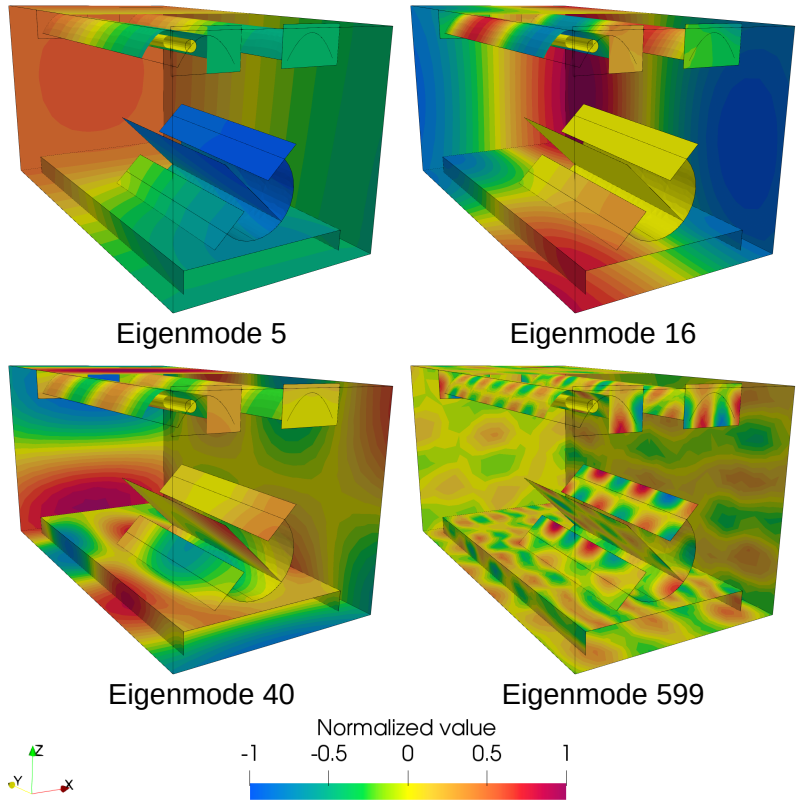

FIGURE 6: Examples of Neumann eigenmodes

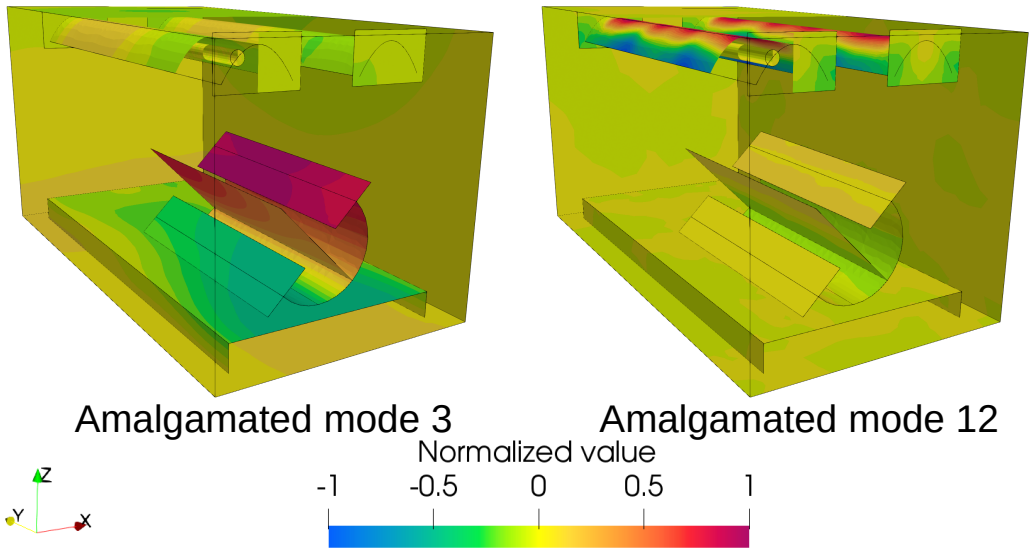

FIGURE 7: Examples of amalgamated modes

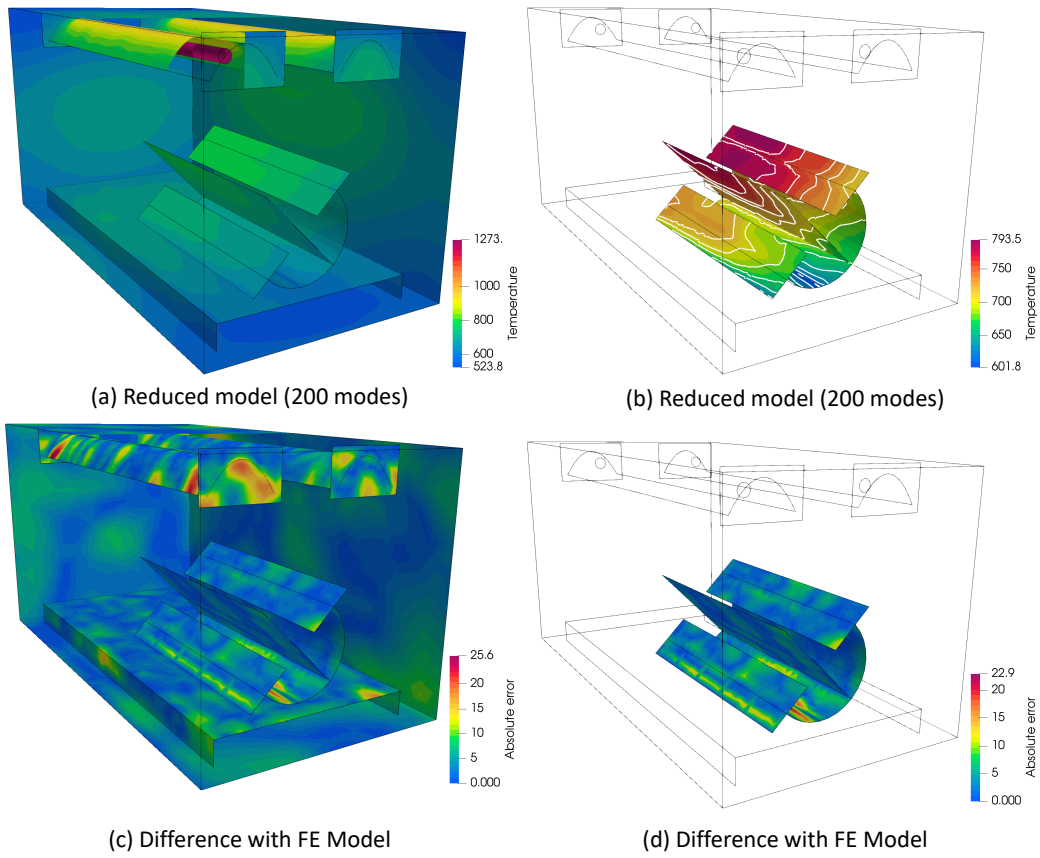

FIGURE 8: Temperature and error fields for scenario 3 at $t = 3\,000\,s$

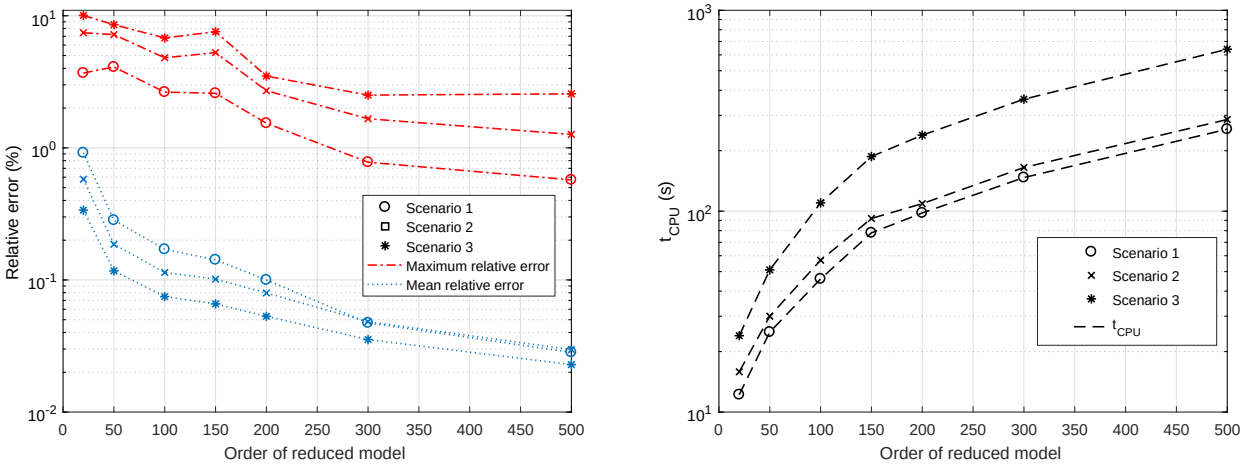

(a) (b)

FIGURE 9: Relative error and CPU time in function of the reduction order